11

Degradation of Nitroaromatic Compounds by Homogeneous AOPs

Fernando S. García Einschlag, Luciano Carlos and Daniela Nichela
Instituto de Investigaciones Fisicoquímicas Teóricas y Aplicadas (UNLP, CCT CONICET), La Plata
Argentina

1. Introduction

Nitroaromatic compounds are environmental contaminants associated with anthropogenic activities such as production and use of dyes, explosives, pesticides and pharmaceuticals. Many of these substances, such as nitrobenzene and nitrophenols, usually found in wastewaters of these industries are considered potentially toxic. Because nitro-substituted aromatic compounds have strong electron withdrawing groups, they are poorly biodegradable by aerobic treatments. The detoxification of wastewaters containing these hazardous substances is very difficult since, due to their high stability, they are usually refractory to conventional biological treatments.

Research on alternative or additional methods of wastewater treatment is of current interest. Wastewater treatment by means of advanced oxidation processes (AOPs) has become one of the issues of major interest in modern environmental chemistry. Various AOPs are nowadays available and applicable at laboratory, pilot or even technical levels for achieving oxidative degradation of organic pollutants in aqueous media. These processes are based on the production of highly reactive species. Among them, the hydroxyl radicals ($HO^{\bullet}$) are the main oxidizing species. Hydroxyl radicals are able to oxidize most organic compounds due to their high reactivity and low selectivity. The reaction of $HO^{\bullet}$ with organic compounds (by addition to double bonds and/or by hydrogen abstraction) generates C-centered radicals that are subsequently trapped by dissolved oxygen to yield peroxides and peroxyl radicals. These intermediates initiate thermal chain autooxidation reactions and the overall processes may, if necessary, lead to complete mineralization. A clear understanding of the effect of reagent concentrations on the evolution of reaction byproducts is critical for producing proper engineering designs. Therefore, the optimization of AOP-methods for waste water treatment requires a comprehensive understanding of the chemical events that govern the transformation rates of the pollutants.

The main objective of this chapter is to provide a comprehensive description of physicochemical phenomena that govern both the transformation rates of nitroaromatic pollutants and the overall degradation efficiencies during waste water treatments by different advanced oxidation processes in homogeneous phase. The chapter summarizes the results obtained in studies related with the degradation of nitroaromatic compounds of environmental relevance by different homogeneous AOPs. Simple tools for describing the

main kinetic features of each system are presented. In addition, the influence of reaction conditions in the transformation pathways of nitrobenzene is discussed.

2. Methods

2.1 Substrate characterization

Physicochemical properties of the organic pollutants (i.e., absorption coefficients, rate constants, and acid-base behavior, among others) should be known to develop reaction models capable of predicting oxidation efficiencies. Speciation of the model pollutants may influence the kinetic trends observed in AOP systems since both the spectral behavior and the reactivity towards $HO^{\bullet}$ radicals depend on speciation. Speciation studies presented include the analysis of acid base and, for Fenton systems, complexation equilibria. In addition, spectral characterization of reaction mixtures is required for evaluating inner filter effects in photoenhanced technologies. Another relevant parameter to be considered is the substrate reactivity towards hydroxyl radicals since it governs the fraction of $HO^{\bullet}$ that effectively attack the model pollutant in a given reaction mixture. Therefore, rate constant values are usually required to evaluate $HO^{\bullet}$ scavenging effects. A brief summary of the basic tools used to characterize important physicochemical properties of the benzoic acid derivatives studied in subsections 3.6.3 and 3.7.2 is given below.

2.1.1 Acid base properties

The absorption spectra of the model substrates were recorded from pH 1.5 to pH 5.5. The values of the first deprotonation constants (pK_{a1}) were estimated by nonlinear fitting of the absorbance versus pH profiles obtained at selected wavelengths (Nichela et al., 2010)

$$f = \alpha_0 \times \left(Abs_P - Abs_D\right) + Abs_D \tag{1}$$

where α_0 are given by 10^{-pH} / (10^{-pKa} + 10^{-pH}), Abs_P are the absorptions of the protonated forms and Abs_D are the absorptions of the deprotonated forms.

2.1.2 Substrate speciation and formation of ferric complexes

In order to characterize the substrate speciation conditional formation constants (K) at pH 3.0 for the 1:1 ferric complexes were estimated by nonlinear fitting of the absorbance versus [Fe(III)] profiles at the maximum wavelengths corresponding to each ferric complex. The following expression was used to obtain K values (Nichela et al., 2010)

$$f = a_o + \Delta\varepsilon \times b \times \frac{\left(K \times \left(M_0 + L_0\right) + 1\right) - \sqrt{\left(K \times \left(M_0 + L_0\right) + 1\right)^2 - 4 \times K^2 \times M_0 \times L_0}}{2K} \tag{2}$$

where a_0 is the absorbance of the initial solution containing the free ligand; M_0 and L_0 are the initial metal and ligand concentrations, respectively; b is the optical path length and $\Delta\varepsilon$ is the difference of absorption coefficients between the complex and the ligand.

2.1.3 Evaluation of rate constants by competition kinetics

The analysis of the consumption profiles of different compounds within the same environment in a competition experiment is a means to evaluate their relative reactivity (Pignatello et al., 1999). Assuming that the substituted benzoic acids (S_i) and a reference

compound (S_{Ref}) are solely decomposed by hydroxyl radicals, the following reactions show the competition for the oxidizing species:

$$\mathbf{HO^{\bullet} + S_i \rightarrow Products \qquad k_i} \tag{3}$$

$$\mathbf{HO^{\bullet} + S_{ref} \rightarrow Products \qquad k_{ref}} \tag{4}$$

Thus, the respective consumption rates can be expressed as

$$\frac{-d[S_i]}{dt} = k_i[HO^{\bullet}][S_i] \quad \Rightarrow \quad \frac{d\ln[S_i]}{dt} = -k_i[HO^{\bullet}] \tag{5}$$

$$\frac{-d[S_{ref}]}{dt} = k_{ref}[HO^{\bullet}][S_{ref}] \quad \Rightarrow \quad \frac{d\ln[S_{ref}]}{dt} = -k_{ref}[HO^{\bullet}] \tag{6}$$

If no assumption for the time dependence of the concentration profile for hydroxyl radicals is made, integration of eqns (5) and (6) yields

$$-\ln\frac{[S_i]_t}{[S_i]_0} = k_i \int_0^t [HO^{\bullet}]\,dt \tag{7}$$

$$-\ln\frac{[S_{ref}]_t}{[S_{ref}]_0} = k_{ref} \int_0^t [HO^{\bullet}]\,dt \tag{8}$$

From the kinetic profiles, measured for the substrate and the reference in a competition experiment, the relative reactivity ($\beta = k_i/k_{ref}$) can be obtained by plotting $\ln[S_i]$ against $\ln[S_{ref}]$ as described elsewhere (García Einschlag et al., 2003). Hence, if k_{ref} is known the absolute rate constant for the different substrates S_i can be calculated as $k_i = \beta \cdot k_{ref}$.

2.2 Monitoring the substrate transformation

Different analytical techniques are used to follow substrate consumption and product formation, among them UV/vis, HPLC-UV/vis, HPLC-MS, GC-MS, selective electrodes (i.e., Cl^- and pH), IC and TOC. The reaction rates calculated from the concentration profiles allow obtaining kinetic information, whereas the analysis of reaction intermediates distributions are used for drawing mechanistic conclusions. Finally, the characterization of the initial toxicity and its evolution by means of toxicity tests is recommended.

2.3 Analysis of product distributions

For a detailed study of the contribution of different reaction channels of substrate degradation it should be taken into account that the initial attack of $HO^{\bullet}$ to nitroaromatic substrates produces hydroxynitrocyclohexadienyl-like radicals (HNCHD·). These radicals subsequently form different primary products through parallel reaction pathways. The yield of the i-th primary product (η_i) is defined as the degraded substrate fraction that converts into the corresponding product (X_i) as a result of the aforementioned reaction steps. As primary products also suffer the attack of $HO^{\bullet}$ radicals, the calculation of η values should be carried out by considering the following expressions describing the kinetic profiles of nitrobenzene (NBE) and its products (Carlos et al., 2008)

$$r_{NBE} = -\frac{d[NBE]}{dt} = -k_{NBE}[HO^{\bullet}][NBE] \quad (9)$$

$$r_i = \frac{d[Xi]}{dt} = \eta_i k_{NBE}[HO^{\bullet}][NBE] - k_i[HO^{\bullet}][X_i] \quad (10)$$

According to eqn (9), $[HO^{\bullet}]$ values can be obtained from measured r_{NBE} values as

$$[HO^{\bullet}] = \frac{r_{NBE}}{k_{NBE}[NBE]} \quad (11)$$

Hence, combining eqns (10) and (11) it is possible to deduce a general expression for η_i

$$\eta_i = \frac{r_i}{r_{NBE}} + \frac{k_i[X_i]}{k_{NBE}[NBE]} \quad (12)$$

If only initial reaction stages are considered, product concentrations are negligible and the second term of eqn (12) can be disregarded. Under these conditions, η_i values can be estimated as $\eta_i^{INI} = r_i^{INI}/r_{NBE}^{INI}$ which is strictly valid in the limit of zero conversion degree. In addition, normalized yields (η^N) may be used to compare the formation pathways of the phenolic products, the normalization factor being the sum of their yields

$$\eta^N{}_i = \frac{\eta_i}{\sum \eta_i} \quad (13)$$

Normalized yields permit a more direct comparison of relative contributions of the pathways that lead to the formation of phenols since their sum is independent from the nitrobenzene fraction transformed into other products.

2.4 Kinetic modeling

In order to obtain quantitative expressions describing simplified reaction models, the application of the steady state approximation for $HO^{\bullet}$ radicals is a very useful strategy. Thus, equations governing the production and fate of $HO^{\bullet}$ radicals (i.e., $r_{Prod}^{HO^{\bullet}}$ & $r_{Cons}^{HO^{\bullet}} = k_{app}^{HO^{\bullet}} \times [HO^{\bullet}]$) should be taken into account. The evaluation of $r_{Prod}^{HO^{\bullet}}$ is presented for both dark and irradiated systems; whereas the $HO^{\bullet}$ scavenging factor, that governs the $HO^{\bullet}$ lifetimes, is calculated by taking into account the main decay pathways.

3. Reaction rates and simplified reaction schemes for homogeneous AOPs

This section presents simplified reaction schemes that allowed to obtain quantitative expressions for the experimental trends in different homogeneous AOP systems.

3.1 UV photolysis

In UV photolysis systems ultraviolet irradiation is directly absorbed by a chemical substrate (S), this process is followed by the decomposition of the excited species transforming the parent compound into one or more products. This transformation may involve homolytic or heterolytic breaking of the chemical bonds. These reactions can be represented as follows

$$\mathbf{S + h\nu \rightarrow S^* \rightarrow Prod} \qquad \mathbf{P_a^S\ \Phi^S} \quad (14)$$

where P_a^S is the rate of photons absorbed by S and Φ^S is the quantum yield of substrate photolysis given by eqn (15) (Braun et al., 1986)

$$\Phi^S = \frac{r^S}{P_a^S} = \frac{-d[S]/dt}{P_0(1-10^{-A^S})} \tag{15}$$

where r^S is the rate of substrate transformation (mol L^{-1} s^{-1}), P_a^S is the rate of photons absorbed by the substrate S (einstein L^{-1} s^{-1}), P_0 is the incident photonic rate (einstein L^{-1} s^{-1}) obtained by actinometry and $A^S = \varepsilon^S.l.[S]$ is the absorbance of S at the wavelength of irradiation. Given that many waste water plants use polychromatic irradiation, polychromatic quantum efficiencies (η_S) are a better parameter for practical purposes. The polychromatic quantum efficiency in these processes may be calculated using eqn (16)

$$\eta^S = \frac{-d[S]/dt}{P_0 \sum_i p_i (1-10^{-A^s{}_i})} \tag{16}$$

where d[S]/dt is the substrate degradation rate obtained from the slope of [S] vs. irradiation time, A_i is the absorbance at the i^{th} irradiation wavelength, P_0, is the total incident photon rate, defined as the number of photons entering the solution per unit time and unit volume, p_i is the probability mass function of the photonic lamp emission and the factor ($1–10^{-Ai}$) accounts for the fraction of photons absorbed by the substrate within the reactor.

In order to test the efficiency of UV photolysis for the treatment of nitroaromatic substrates, aqueous solutions of 1-chloro-2,4-dinitrobenzene (CDNB); 2,4-dinitrophenol (DNP); nitrobenzene (NBE); 3-nitrophenol (MNP) and 4-nitrophenol (PNP) were irradiated at pH 2.5 using an HPK125 medium-pressure mercury arc lamp (García Einschlag et al., 2002b). In all cases, the conversion degrees of the different substrates were less than 4% after continuous irradiation for 2-3 h. Polychromatic quantum efficiencies were in the range 1.3×10^{-4}-7.8×10^{-4}. These results are in agreement with reported quantum yields of photolysis of various aromatic compounds that have been determined to be in the range 10^{-3} - 10^{-4} (Lipczynska-Kochany and Bolton, 1991; Lopez et al., 2000). Given the low values obtained for η_S, it is clear that UV photolysis is a rather inefficient method for treating nitroaromatic compounds in waste water.

3.2 VUV photolysis

Water strongly absorbs at irradiation wavelengths shorter than 190 nm, the absorption cross section increasing as the wavelength decreases between 190 and 160 nm (Heit et al., 1998). The VUV photolysis of water may be described by the following processes

$$\mathbf{H_2O + } h\nu \rightarrow \mathbf{H^{\bullet} + HO^{\bullet}} \qquad \mathbf{P_a^{H2O}\,\Phi^{H^{\bullet}}} \tag{17}$$

$$\mathbf{H_2O + } h\nu \rightarrow \mathbf{H^{+} + HO^{\bullet} + e^{-}_{aq}} \qquad \mathbf{P_a^{H2O}\,\Phi^{e-}} \tag{18}$$

where P_a^{H2O}, $\Phi^{H^{\bullet}}$ and Φ^{e-} are the rate of photons absorbed by water, the quantum yield of $H^{\bullet}$ formation and the quantum yield of e- formation, respectively. It is important to recall that, given the high cross section of water molecules within the irradiation wavelength range, $P_a^{H2O} = P_0$. The quantum yield for the production of solvated electrons is low (0.05) and almost wavelength independent. In contrast, values of 0.42 and 0.33 at 172 and 185 nm, respectively, have been reported (Heit et al., 1998) for the quantum yield of $HO^{\bullet}$ production

($\Phi^{HO\bullet}$). In aerated solutions, H atoms and hydrated electrons are efficiently trapped by dissolved oxygen, yielding hydroperoxyl radicals ($HO_2^\bullet$) and its conjugated base, the superoxide anion ($O_2^{\bullet-}$). Since the latter species are much less reactive than hydroxyl radicals, the main pathway leading to the substrate decomposition is given by rxn (19)

$$\mathbf{S + HO^\bullet \rightarrow Prod \qquad k_S} \tag{19}$$

The degradation of the substrate 4-chloro-3,5-dinitrobenzoic acid (CDNBA) by VUV process was studied (Lopez et al., 2000) with two VUV irradiation sources, a low pressure mercury arc with Suprasil envelope allowing irradiation at 185 nm and a xenon-excimer lamp emitting at 172 nm.

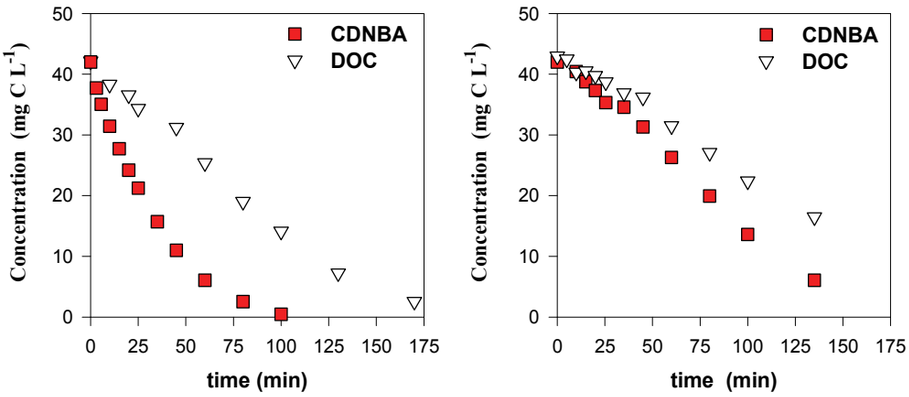

Fig. 1. Degradation of CDNBA by VUV photolysis of water. Left: 172 nm. Right: 185 nm.

Fig. 1a shows that irradiation of aerated aqueous solutions of CDNBA using the Xe-excimer lamp resulted in a relatively fast CDNBA degradation and an efficient mineralization within the first three hours. The disappearance of CDNBA and the DOC depletion were slightly slower under VUV irradiation at 185 nm than at 172 nm (Fig. 1b). The initial rates of CDNBA disappearance (r^S) were used to obtain the apparent quantum yields of substrate disappearance at each wavelength

$$\Phi^S_{app} = \frac{r^S}{P_0} \tag{20}$$

the initial Φ^S_{app} values being 1.1×10^{-2} and 0.90×10^{-2} at 172 and 185 nm, respectively. This slightly lower value of Φ_{CDNBA} may result from the lower $\Phi_{HO\bullet}$ at 185 nm than at 172 nm. The efficiency of $HO^\bullet$ radicals trapping by CDNBA was obtained from ratio of Φ_{CDNBA} and $\Phi_{HO\bullet}$ values. The low value obtained at both wavelengths (approx. 0.025) is related to the limited penetration of the VUV radiation in water. Relative high concentrations of short lived $HO^\bullet$ radicals are formed in a narrow layer around the lamp shaft, thus diffusion is not fast enough to avoid depletion of the substrate and molecular oxygen in this layer.

3.3 UV/H_2O_2 systems

In the UV/H_2O_2 process, the photolysis of H_2O_2 results in the homolysis of the oxygen-oxygen bond and the production of hydroxyl radicals ($HO^\bullet$).

$$H_2O_2 + h\nu \rightarrow 2\,HO^{\bullet} \qquad P_a^{H2O2}\,\Phi^{H2O2} \tag{21}$$

where P_a^{H2O2} is the rate of photons absorbed by H_2O_2 and Φ^{H2O2} is the quantum yield of H_2O_2 photolysis. Techniques based on the use of H_2O_2 are advantageous (Stefan et al., 1996) since H_2O_2 can be readily mixed with water in all proportions and costs associated to production and handling of H_2O_2 are not high. This process leads, in most cases, to the mineralization of the organic substrate, i.e. production of CO_2, H_2O, and mineral acids.

We studied the degradation of the substrates CDNBA, CDNB, DNP, MNP, NBE and PNP by the UV/H_2O_2 process (García Einschlag et al., 2002a; García Einschlag et al., 2002b). Dramatic changes in the absorption spectra were observed indicating that nitroaromatic substrates are rapidly consumed under these conditions. The degradation rates were strongly dependent on substrate and H_2O_2 concentrations. The initial rates of substrate disappearance (r=-d[S]/dt) under different conditions show that when increasing the concentration of H_2O_2, a maximum rate (r_{max}) could be observed. When increasing the initial substrate load $[S]_0$, the optimal H_2O_2 concentration ($[H_2O_2]_{OPT}$, defined as the initial H_2O_2 concentration for which r_{max} was reached) increased proportionally. Fig. 2 shows the behavior of the r/r_{max} represented as a function of the parameter $\boldsymbol{R}$ (defined as $[H_2O_2]_0/[S]_0$).

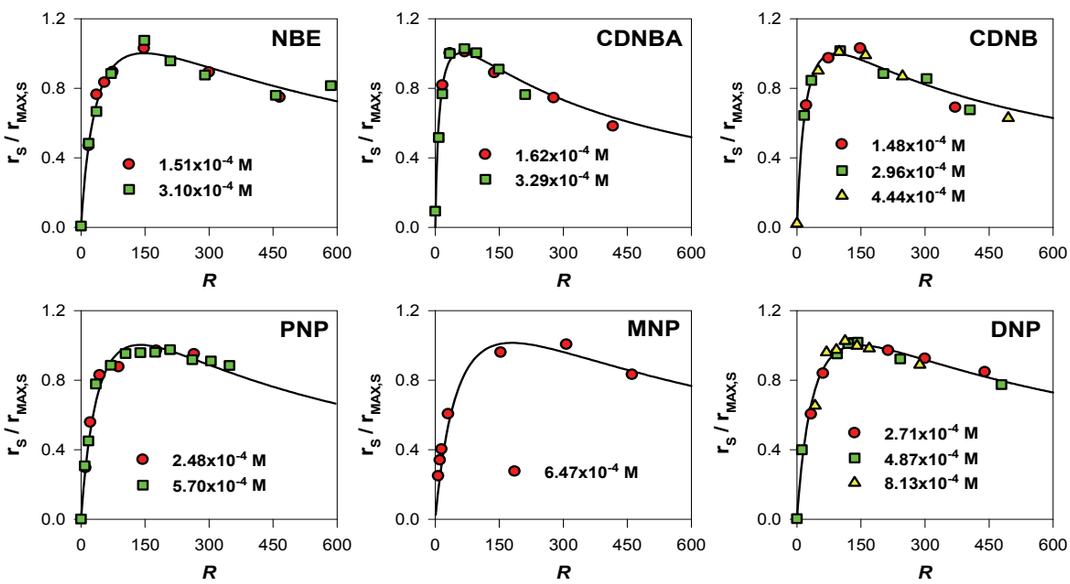

Fig. 2. Normalized initial consumption rates for the different substrates in UV/H_2O_2 processes.

Interestingly, optimal concentration ratios R_{OPT} (=$[H_2O_2]_{OPT}/[S]_0$) were independent of $[S]_0$. As $[H_2O_2]_0$ increased for a given $[S]_0$, a remarkable change in the initial rate was observed, but when $R > R_{OPT}$, this rate showed a smooth decrease. This behavior is of great importance from both a practical and an economical point of view, since there is a wide range of R values corresponding to oxidation rates of at least 90% of the optimal rate.

The degradation of pollutants by the UV/H_2O_2 technique involves a complex set of reactions. Although a detailed analysis of all the reactions involved in the oxidative degradation manifold of each compound is a very difficult task (Glaze et al., 1995; Stefan and Bolton, 1998; Crittenden et al., 1999; Stefan et al., 2000), the general trends observed are

very similar (Fig. 2). Hence, we proposed a simple kinetic model for describing the observed behavior (García Einschlag et al., 2002b). During the initial oxidation stages, only S and H_2O_2 are present in substantial amounts. Accordingly, the $HO^\bullet$ radicals generated by H_2O_2 photolysis rxn (21) may be trapped either by the substrates rxn (19) or by H_2O_2 rxn (22)

$$\mathbf{H_2O_2 + HO^\bullet \rightarrow HO_2^\bullet + H_2O} \qquad \mathbf{k_{H2O2}} \tag{22}$$

Reactions implying $HO_2^\bullet$ or $O_2^{\bullet-}$ have not been considered, as their reactivity is much lower than that of $HO^\bullet$ (Simic, 1975; Nadezhdin and Dunford, 1979; Getoff, 1997). A similar remark applies to the reactions associated with the intermediate products, whose concentrations during the first irradiation stages may be neglected. UV photolysis of the substrates was also disregarded (see section 3.1).

3.3.1 Initial degradation rates under monochromatic irradiation

According to the reduced set of reactions proposed, the substrate consumption rate (r) is governed by

$$r = \frac{-d[S]}{dt} = k_S\,[S][HO^\bullet] \tag{23}$$

Assuming that the steady-state hypothesis holds for $HO^\bullet$, their concentration is given by

$$[HO^\bullet] = \frac{r_{HO^\bullet}}{k_{H_2O_2}\,[H_2O_2] + k_S\,[S]} \tag{24}$$

where r_{HO} stands for the rate of $HO^\bullet$ production. Under monochromatic irradiation, r_{HO} may be expressed as

$$r_{HO^\bullet} = \frac{2\,P_0\,\Phi^{H_2O_2}\,(1 - 10^{-A})\,\varepsilon^{H_2O_2}\,[H_2O_2]}{\varepsilon^{H_2O_2}\,[H_2O_2] + \varepsilon^{S}\,[S]} \tag{25}$$

where $(1\text{-}10^{\text{-}A})[(\varepsilon_{H2O2}[H_2O_2])/(\varepsilon_{H2O2}[H_2O_2] + \varepsilon_S c_S)]$ is the fraction of photons absorbed by H_2O_2. Combining eqns (23), (24) and (25) and assuming absorbance values greater than 2, the oxidation rate of the substrate (r) may be expressed as (García Einschlag et al., 2002b)

$$r = \frac{2\,P_0 \Phi^{H_2O_2} \varepsilon\,R}{(\varepsilon\,R + 1)\,(k\,R + 1)} \tag{26}$$

where $R=[H_2O_2]_0/[S]_0$, $\varepsilon=\varepsilon_{H2O2}/\varepsilon_S$ and $k=k_{H2O2}/k_S$. The optimal ratio R_{OPT} leading to the highest initial rate can be obtained by differentiation of eqn (26) (i.e. $R=R_{OPT}$ for $dr/dR=0$)

$$R_{OPT} = \sqrt{\frac{1}{k\,\varepsilon}} = \sqrt{\frac{k_S\,\varepsilon^S}{k_{H_2O_2}\,\varepsilon^{H_2O_2}}} \tag{27}$$

This simple expression of R_{OPT} ($=[H_2O_2]_{OPT}/[S]_0$) might be used, either to evaluate $[H_2O_2]_{OPT}$ if k_S and ε_S are known or to estimate k_S if $[H_2O_2]_{OPT}$ is determined experimentally. The validity of eqns (26) and (27) was tested by comparing experimental and simulated trends of the oxidation rates. Solid lines in Fig. 2 were calculated using eqn (26).

3.3.2 Initial degradation rates under polychromatic irradiation

The previous ideas can be extended to processes induced by polychromatic irradiation sources. A typical HPK125 lamp exhibits a continuous background and various emission lines. Therefore, the rate of photon absorption by hydrogen peroxide, P_a^{H2O2}, is described by

$$P_a^{H_2O_2} = P_0 \int_\lambda \frac{(1 - 10^{-A_\lambda})\,\varepsilon_\lambda^{H_2O_2}\,[H_2O_2]}{\varepsilon_\lambda^{H_2O_2}\,[H_2O_2] + \varepsilon_\lambda^{S}\,[S]} p_\lambda d\lambda \tag{28}$$

where the quantity A_λ represents the total absorbance of the solution, $\varepsilon_\lambda^{H2O2}$ and ε_λ^{S} are the molar absorption coefficients of substrate and H_2O_2 at a given wavelength, and p_λ is the probability density function of the photonic emission. Although this integral cannot be solved in a simple way, the calculation of P_{H2O2} can be carried out as a discrete sum. Eqn (28) was solved for the wavelength range between 200 and 500 nm

$$P_{H_2O_2} = P_0 \sum_i p_i (1 - 10^{-A_i}) \frac{\varepsilon_i^{H_2O_2}\,[H_2O_2]}{\varepsilon_i^{H_2O_2}\,[H_2O_2] + \varepsilon_i^{S}\,[S]} \tag{29}$$

where subscript i refers to a very small finite wavelength interval (i.e., 1 nm) and p_i is the probability mass function of the photonic emission of the lamp. Thus, the expression equivalent to eqn (26) under polychromatic irradiation turns out to be

$$r_S = \frac{2\,P_0}{(k\,R + 1)} \sum_i \frac{p_i\,\Phi_i^{H_2O_2}\,\varepsilon_i\,R}{(\varepsilon_i\,R + 1)} \tag{30}$$

where $\varepsilon_i = \varepsilon_i^{H2O2}/\varepsilon_i^{S}$. As already indicated r_S exhibits a maximum at R_{OPT}. After setting $dr_S/dR = 0$ the following expression can be obtained (García Einschlag et al., 2002a)

$$\sum_i \frac{p_i\,\Phi_i^{H_2O_2}\,\varepsilon_i}{(\varepsilon_i\,R_{OPT} + 1)^2} = k \sum_i \frac{p_i\,\Phi_i^{H_2O_2}\,\varepsilon_i^{2}\,R_{OPT}^{2}}{(\varepsilon_i\,R_{OPT} + 1)^2} \tag{31}$$

It is clear that the latter equation cannot be rearranged to obtain R_{OPT} since it is an implicit equation (in R_{OPT}). In order to obtain an expression for R_{OPT} we defined the quantity $f(i)$ as

$$f(i) = \frac{p_i\,\Phi_i^{H_2O_2}\,\varepsilon_i}{(\varepsilon_i\,R_{OPT} + 1)^2} \tag{32}$$

which is a function of the spectral and kinetic properties of the system. Eqn (31) may be rearranged to give (García Einschlag et al., 2002a)

$$R_{OPT} = \sqrt{\frac{k_S}{k_{H_2O_2}} \left\langle \frac{\varepsilon^{H_2O_2}}{\varepsilon^{S}} \right\rangle^{-1}} \tag{33}$$

where $\langle \varepsilon^{H2O2}/\varepsilon^{S} \rangle$ is the statistical expectance of the ratio $\varepsilon_i^{H2O2}/\varepsilon_i^{S}$, the quantity $f(i)$ being the probability distribution function. Although eqn (33) does not allow the calculation of R_{OPT}, it is interesting to note its similarity with eqn (27) derived for monochromatic irradiation.

3.4 UV/NO_3^- and UV/NO_2^- systems

The photolysis mechanisms of nitrous acid, nitrite and nitrate involve photolytic pathways that result in the formation of HO• and nitrogen species such as •NO, •NO_2 and $ONOO^-$, as primary photoproducts (Mark et al., 1996; Mack and Bolton, 1999; Goldstein and Rabani, 2007). The primary photoprocesses and the main subsequent reactions leading to the production of HO• in acidic media are

Nitrous acid/nitrite systems

$$HNO_2 + h\nu \rightarrow HO^\bullet + {}^\bullet NO \qquad P_a^{HNO2}\Phi^{HO^\bullet} \tag{34}$$

$$NO_2^- + h\nu \rightarrow O^{\bullet-} + {}^\bullet NO \xrightarrow{H^+} HO^\bullet + {}^\bullet NO \qquad P_a^{NO2-}\Phi^{HO^\bullet} \tag{35}$$

Nitrate systems:

$$NO_3^- + h\nu \rightarrow ONOO^- \xrightarrow{H^+} ONOOH \qquad P_a^{NO3-}\Phi^{PNA} \tag{36}$$

$$ONOOH \rightarrow (NO_3^- + H^+)_{72\%} + (HO^\bullet + {}^\bullet NO_2)_{28\%} \qquad k_{PNA} \tag{37}$$

$$NO_3^- + h\nu \rightarrow O^{\bullet-} + {}^\bullet NO_2 \xrightarrow{H^+} HO^\bullet + {}^\bullet NO_2 \qquad P_a^{NO3-}\Phi^{HO^\bullet} \tag{38}$$

Among the photogenerated species, HO• is much more reactive and less selective than other primary photoproducts and peroxynitrite is unstable in acid media (Goldstein et al., 2005). Consequently, the kinetic behavior of many UV/HNO_2/NO_2^- and UV/NO_3^- systems is expected to be dominated by the production and fate of hydroxyl radicals.

We have studied the degradation of the substrates NBE and PNP by using UV irradiation in the presence of HNO_2/NO_2^- or NO_3^- as sources of HO• radicals at pH 3.0 (García Einschlag et al., 2009). It was found that both methods are capable of destroying the substrates within a few hours. The concentration profiles obtained by HPLC analyses follow pseudo-first-order kinetics for both substrates during several minutes of irradiation.

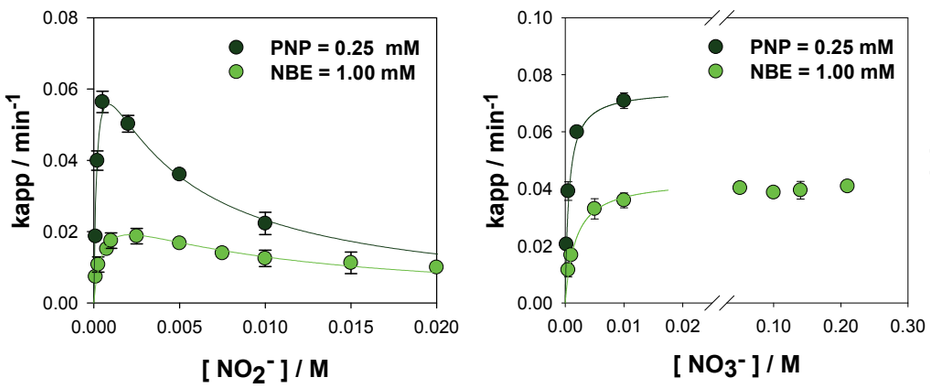

Fig. 3. Dependence of k_{app} values for PNP and NBE degradation on additive concentrations.

The initial apparent rate constants (k_{app}) were found to depend on both the substrate and additive (I= HNO_2/NO_2^- or NO_3^-) concentrations. In all cases, k_{app} decreased with increasing initial substrate concentration. The dependencies of k_{app} for PNP and NBE on the initial additive concentration for both UV/HNO_2/NO_2^- and UV/NO_3^- systems are shown in Fig. 3.

3.4.1 UV/HNO_2/NO_2^- systems

Similarly to the behavior observed for UV/H_2O_2 systems, the apparent rate constants of NBE and PNP degradation induced by HNO_2/NO_2^- photolysis show a maximum value and then decrease with increasing additive concentration (Fig. 3a). As in UV/H_2O_2 systems, this decrease in the apparent rate constant of substrate degradation is due to a scavenging effect of HO• by the additive (similar scavenging effects have already been reported (Vione et al., 2004)). For the same additive concentration, higher values of k_{app} are observed for PNP, the substrate present in lower concentration. In addition, the highest PNP and NBE degradation rates are observed for HNO_2/NO_2^- concentrations of 0.9 mM and 2.1 mM, respectively. This result correlates well with the increase of the optimal additive concentration with substrate loading observed for UV/H_2O_2 systems. By contrast, rather low optimal ratios (R_{OPT} = $[I]_{OPT}/[S]$) were observed (*i.e.* 3 for PNP and 2 for NBE) in comparison with those reported for UV/H_2O_2 systems (*i.e.* 160 for PNP and 150 for NBE) (García Einschlag et al., 2002b).

3.4.2 UV/NO_3^- systems

The study of the effect of NO_3^- concentration on k_{app} yielded plots (Fig. 3b) with shapes that diverge from the trends observed in UV/HNO_2/NO_2^- and UV/H_2O_2 systems, since no decrease of k_{app} values was observed even at very high NO_3^- concentrations. This result reveals that the effectiveness of NO_3^- as HO• scavenger is negligible due to the small value of the related rate constant (Mack and Bolton, 1999).

3.4.3 Simplified reaction model

The model proposed for UV/H_2O_2 systems can be easily extended to the UV/HNO_2/NO_2^- and UV/NO_3^- systems. The most important reactions involving the additives (I) may be represented as (García Einschlag et al., 2009)

$$\mathbf{I + h\nu \rightarrow HO^{\bullet} + PR^{\bullet}} \qquad \mathbf{\int P^{\lambda}_{Abs,I}\, \Phi^{\lambda}_{I \rightarrow HO^{\bullet}}} \tag{39}$$

$$\mathbf{I + HO^{\bullet} \rightarrow SR^{\bullet}} \qquad \mathbf{k_I} \tag{40}$$

where I represents the photoactive species (*i.e.*HNO_2/NO_2^-, NO_3^- or H_2O_2) capable of generating HO• radicals, PR• denotes primary radicals accompanying HO• generation (*i.e.* •NO, •NO_2 or HO•) and SR• are radicals produced by HO• attack towards the photoactive species (*i.e.* •NO_2, •NO_3 or HO_2•). In addition, $P^{\lambda}_{Abs,I}$ is the rate of photons absorbed by the additive I at a given wavelength of irradiation, $\Phi^{\lambda}_{I \rightarrow HO^{\bullet}}$ is the wavelength dependent quantum yield of HO• photoproduction and k_I is the bimolecular rate constant for the reaction of hydroxyl radicals with the photoactive species. As in the case of UV/H_2O_2 systems, reactions of the primary (PR•) and secondary (SR•) radicals as well as the reactions associated with the intermediate products may be neglected. Assuming steady-state conditions for HO• radicals, an expression similar to eqn (24) can be obtained. In order to evaluate the rate of HO• production in UV/I systems, the following expression can be used

$$r_{Prod,HO^{\bullet}} = P_0 \sum_{\lambda} \Phi^{I \rightarrow HO^{\bullet}}_{\lambda} \times (1 - 10^{-A_{\lambda}}) \times \frac{\varepsilon^{I}_{\lambda}[I]}{\varepsilon^{I}_{\lambda}[I] + \varepsilon^{S}_{\lambda}[S]} \times p_{\lambda} \tag{41}$$

Hence, the initial apparent rate constant of substrate consumption is given by

$$k_{app} = \frac{P_0}{\frac{k_I}{k_S}[I] + [S]} \sum_{\lambda} \frac{\Phi_{\lambda}^{I \to HO^{\bullet}} (1 - 10^{-A_{\lambda}})[I]}{[I] + \frac{\varepsilon_{\lambda}^{S}}{\varepsilon_{\lambda}^{I}}[S]} p_{\lambda} \quad (42)$$

Replacing the summation with a factor of the form [I]/([I] + c[S]) and using R in place of [I]/[S], the latter equation may be approximated by

$$k_{app} \cong \frac{a \times R}{[S] \times (bR + 1) \times (R + c)} \quad (43)$$

where the parameter "a" depends on both the incident photon rates and the polychromatic quantum efficiencies.

Equation (43) is a rough approximation of k_{app} that may be used to account for the trends observed. Nonlinear fitting was used to obtain the parameters "b" and "c" for the substrates NBE and PNP in the UV/HNO_2/NO_2^-, UV/NO_3^- and UV/H_2O_2 systems (García Einschlag et al., 2009). Although the constants obtained have no straightforward physical interpretation, the parameter "b" is mainly related to the ratio of rate constants k_I/k_S, whereas the parameter "c" may be considered as an effective value for the relative absorption coefficient. The solid lines in Fig. 3 show that the model is capable of describing the observed trends. The analysis of "b" values obtained with eqn (43) are in reasonable agreement with reported bimolecular rate constants (Buxton et al., 1988). On the other hand, the values obtained for parameter "c" reflect the fact that average inner filter effects are much more noticeable for UV/H_2O_2 systems than for UV/HNO_2/NO_2^- and UV/NO_3^- systems. Thus, the trends experimentally observed for k_{app} against the concentration of $HO^{\bullet}$ photoproducers may be rationalized by considering two opposite effects. The increase of additive concentrations increases the amount of photons absorbed by the photoactive species whereas high additive concentrations may either result in significant decreases of the degradation rates or not, depending on the additive's ability to trap hydroxyl radicals.

3.5 Fenton systems

It is generally accepted that, in Fenton systems, the most important reactive species are hydroxyl radicals, produced by interaction of H_2O_2 with ferrous ions in acid media (Pignatello et al., 2006)

$$\mathbf{Fe^{2+} + H_2O_2 \rightarrow Fe^{3+} + HO^{\bullet} + HO^-} \qquad \mathbf{k_{Fe+2}} \quad (44)$$

The removal of organic compounds in reaction mixtures starting with Fe^{2+} and having H_2O_2 in large stoichiometric excess (10 to 100 peroxide-to-iron molar ratio) generally exhibits an initial fast degradation phase due to the high amount of $HO^{\bullet}$ produced by rxn (44). Subsequently, a much slower phase is usually observed (where the reduction of Fe^{+3} is rate-limiting (De Laat and Gallard, 1999)). The extent of each phase usually depends on the iron/organic compound molar ratio (Chan and Chu, 2003). We studied the degradation of NBE using the Fenton reagent in different experimental conditions (Carlos et al., 2008). Fig. 4 shows the concentration profiles obtained in a representative experiment for NBE and the primary phenolic derivatives.

3.6 Fenton-like systems

Fenton-like processes involve a series of thermal reactions catalyzed by transition metal salts (ferric and cupric salts, among others) that lead to H_2O_2 decomposition. In addition to the

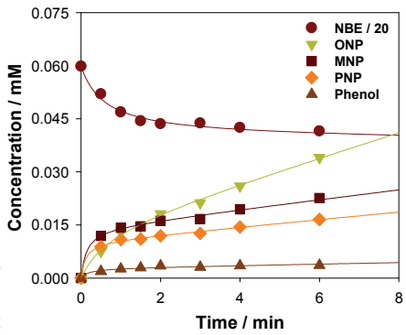

Fig. 4. Kinetic profiles of NBE and its primary phenolic products obtained in Fenton treatment.

oxidation of Fe^{+2} by H_2O_2 rxn (44), ferric ions can also react with H_2O_2 through rxn (45) thereby regenerating Fe^{2+} and supporting the Fenton process (Walling, 1975)

$$\mathbf{Fe^{3+} + H_2O_2 \rightarrow Fe^{2+} + HO_2^{\bullet} + H^+ \quad k_{Fe+3}} \tag{45}$$

In the absence of organic matter, the latter reaction is rate limiting for H_2O_2 decomposition since the rate constant for rxn (44) is about 4 orders of magnitude higher than that of rxn (45). However, it has been established that organic compounds can remarkably affect the kinetics of H_2O_2 decomposition, because they can significantly increase the rates of chain propagation steps. It has been reported (Chen and Pignatello, 1997) that catalytic amounts of quinone-like intermediates (QLH_2 and $QLH^{\bullet}$) enhance organic matter oxidation since they can readily accelerate the reduction of ferric species to ferrous species.

$$\mathbf{Fe^{3+} + QLH_2 \rightarrow Fe^{2+} + QLH^{\bullet} + H^+} \tag{46}$$

$$\mathbf{Fe^{3+} + QLH^{\bullet} \rightarrow Fe^{2+} + QL + H^+} \tag{47}$$

Given the complexity of Fe^{3+}/H_2O_2 systems, many variables may significantly influence the efficiency and the economic competitiveness of these techniques.

3.6.1 Autocatalytic concentration profiles

We have studied NBE oxidation kinetics in excess of H_2O_2 and catalytic concentrations of Fe^{3+} (Nichela et al., 2008). We found that NBE kinetic profiles display an autocatalytic behavior with an initial ''slow phase'', where [NBE] slightly decreases at a practically constant rate for conversion degrees lower than 10%, followed by a ''fast phase'' where the process is substantially accelerated obeying pseudo first-order kinetics. A typical concentration profile is presented in Fig. 5. The complex consumption profiles were analyzed by calculating the rates during the slow phase (r^{NBE}_{slow}), the average rates of the fast phase (r^{NBE}_{fast}), the apparent pseudo first-order rate constants for the fast phase (k^{NBE}_{fast}), and the transition times from the slow to the fast phase (t_{tr}^{NBE}). The slopes fitted for NBE consumption throughout each phase and the transition time, obtained by the intersection of the straight lines linked to each phase, are depicted in Fig. 5.

Although Fenton-like processes may involve very complex reaction mechanisms (Pignatello et al., 2006) a reduced set of reactions allow explaining the experimental trends observed (Nichela et al., 2008). The organic matter oxidation is induced by hydroxyl radicals produced through rxn (44). According to the value of k_{Fe+2} and the typical [H_2O_2] used in

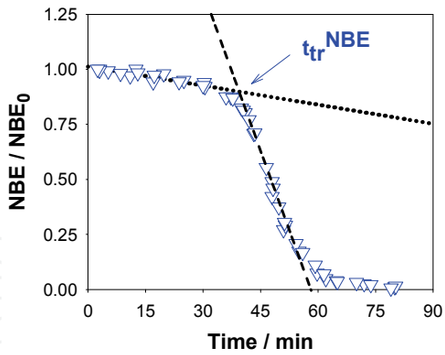

Fig. 5. Normalized autocatalytic profiles obtained for NBE in Fenton-like systems.

Fenton-like systems, the overall reaction rates are mainly controlled by the reduction of Fe^{3+} to Fe^{2+}. The autocatalytic profiles can be explained considering that during the first reaction stages the rate limiting step is Fe^{2+} production via rxn (45). This is supported by the dependence of $r^{NBE}{}_{slow}$ on $[Fe^{3+}]_0$ and $[H_2O_2]_0$. As the reaction advances, quinone-like species such as hydroquinone, semiquinone radical and structurally related nitro-derivatives are generated. Some of these aromatic intermediates can provide alternative pathways for Fe^{3+} reduction such as rxns (46) and (47), thereby promoting the global acceleration of the process (Chen and Pignatello, 1997).

During the initial phase only a 10% of NBE is consumed, however this phase covers more than 50% of the time required for complete NBE oxidation. Thus, from a technical viewpoint it is wise to perform a detailed analysis of the reaction rates for the slow phase. In order to describe several kinetic features, the parameter $z^{NBE}{}_{slow}$ was used (Nichela et al., 2008)

$$z_{Slow}^{NBE} \equiv \frac{r_{Slow}^{NBE}}{[NBE]_0} \tag{48}$$

Hence, $z^{NBE}{}_{slow}$ corresponds to NBE oxidation rate during the slow phase relative to $[NBE]_0$. It was experimentally observed that $z^{NBE}{}_{slow}$ increases with $[H_2O_2]_0$ and $[Fe^{3+}]_0$ but decreases with $[NBE]_0$, within the analyzed concentration range. In addition, as $z^{NBE}{}_{slow}$ increases, the transition time towards the fast phase diminishes. Figure 6 shows linear dependencies among functions of $z^{NBE}{}_{slow}$ and [NBE], $[Fe^{3+}]$, $[H_2O_2]$ and $t_{tr}{}^{NBE}$ values.

3.6.2 Simplified model for the slow phase

The increase of $r^{NBE}{}_{slow}$ with $[H_2O_2]_0$ and $[Fe^{3+}]_0$ may be ascribed to an enhanced $HO^{\bullet}$ production by reactions (44) and (45). On the other hand, an increase of NBE concentration diminishes the steady-state concentration of hydroxyl radicals by scavenging effect through rxn (19), resulting in lower $z^{NBE}{}_{slow}$ values. Neglecting the effect of organic byproducts during early reaction stages, reactions (19), (22), (44) and (45) can be considered as the key steps of the slow phase. As a result, simple equations for $r_{Slow}{}^{NBE}$ and $r_{Slow}{}^{H2O2}$ can be deduced assuming steady-state for Fe^{2+} and $HO^{\bullet}$

$$[Fe^{2+}]_{Slow} \cong \frac{k_{Fe^{+3}}}{k_{Fe^{+2}}}.[Fe^{3+}] \cong \frac{k_{Fe^{+3}}}{k_{Fe^{+2}}}.[Fe^{3+}]_0 \tag{49}$$

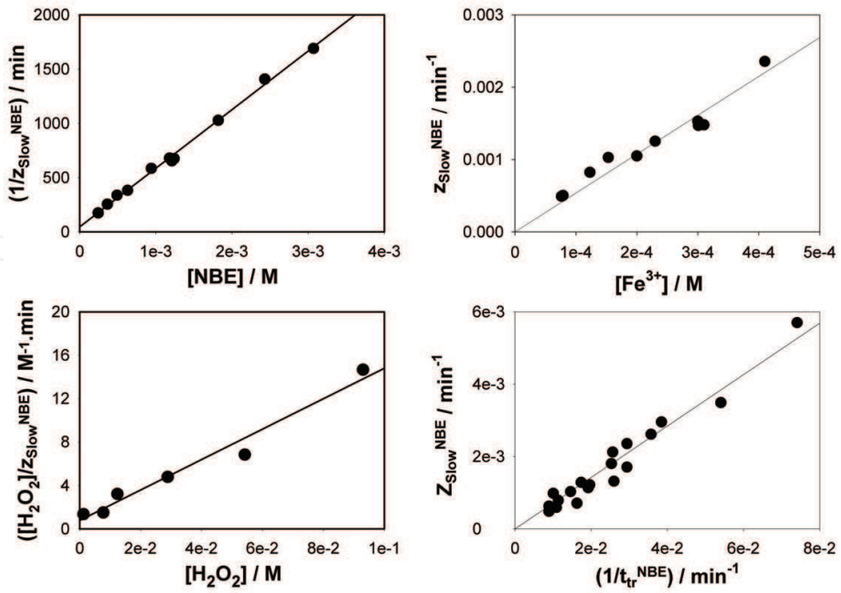

Fig. 6. Linear relationships among functions of z^{NBE}_{slow} and different parameters

$$[HO^{\bullet}]_{Slow} \cong \frac{k_{Fe^{+2}}.[Fe^{2+}]_{ss}.[H_2O_2]}{k_{NBE}.[NBE]+k_{H_2O_2}.[H_2O_2]} \tag{50}$$

Given that $k_{Fe+3} << k_{Fe+2}$, during the slow phase the Fe^{2+} concentration is negligible and $[Fe^{3+}]_{slow} \approx [Fe^{3+}]_0$. By combining the rate equations for NBE and H_2O_2 with eqns (49) and (50), the following expressions for the slow phase can be obtained (Nichela et al., 2008)

$$r^{NBE}_{Slow} = k_1.[Fe^{3+}].[H_2O_2]\left\{\frac{k_{NBE}.[NBE]}{k_{NBE}[NBE]+k_{HP}[H_2O_2]}\right\} \tag{51}$$

$$r^{HP}_{Slow} = k_1.[Fe^{3+}].[H_2O_2].\left\{2+\frac{k_{HP}.[H_2O_2]}{k_{NBE}[NBE]+k_{HP}[H_2O_2]}\right\} \tag{52}$$

It is worth to mention that eqns (51) and (52) are in excellent agreement with the experimental trends, as it is observed in Fig. 6.

3.6.3 Semi quantitative analysis of the autocatalytic profiles

We also used Fenton-like process for the oxidation of a series of structurally related substrates, in order to test the autocatalytic nature of these systems (Nichela et al., 2010). The model compounds were 2-hydroxybenzoic (2HBA), 2,4-dihydroxybenzoic (24DHBA), 2-hydroxy-5-nitrobenzoic (2H5NBA), 4- hydroxy-3-nitrobenzoic (4H3NBA) and 2- hydroxy-4-nitrobenzoic (2H4NBA) acids. The normalized profiles of [S] and $[H_2O_2]$ are shown in Fig. 7. The kinetic behavior is strongly dependent on the nature of the substrate and, excepting 4H3NBA, the substrates clearly display autocatalytic decays, the profiles being like inverted S-shaped curves. The quantitative description of this kinetic traces is rather complicated and, to the best of our knowledge, no simple equation has been proposed to model

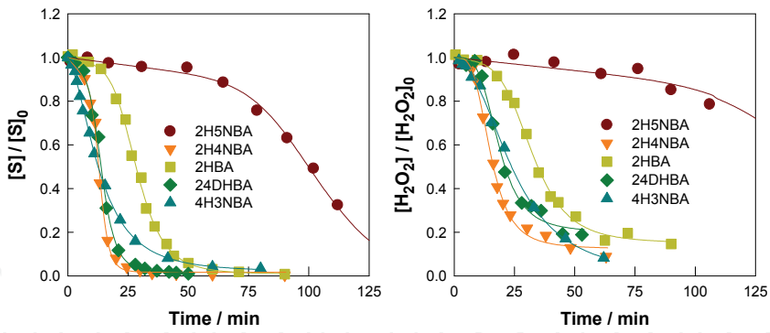

Fig. 7. Normalized concentration profiles of model substrates obtained in dark Fenton-like process.

concentration profiles of this kind that are frequently found in degradation studies of environmental relevance. For the quantitative comparison of the kinetic curves we proposed an empirical equation for fitting the normalized decay profiles (Nichela et al., 2010)

$$f = \frac{(1 - a \times t - d)}{1 + (t/b)^c} + d \tag{53}$$

In this equation, the parameters a, b, c and d may be employed to characterize the average oxidation rate during the slow phase (the normalized initial rate), the time required to reach half of the initial concentration (the apparent half-life), the average slope during the fast phase and the final residual value, respectively. The solid lines in Fig. 7 show that eqn (53) allows a precise estimation of the temporal dependence of concentration profiles. Although the chemical structures of the substrates are closely related, the degradation timescales are remarkably different. During early reaction stages, the depletion rates follow the trend 4H3N-BA > 2H4N-BA ≈ 24DH-BA > 2H-BA >> 2H5NBA. It should be noted that, despite lacking a precise kinetic meaning, eqn (53) has a key advantage from a practical point of view: it requires only a few experimental points to draw S-shaped curves that closely describe the complex autocatalytic profiles frequently observed in Fenton-like systems.

3.7 Photo-Fenton systems

The strategy most frequently used in Fenton systems to increase the reaction rates and improve the mineralization efficiencies is the use of UV and/or visible irradiation. The enhancement is mostly due to the photolysis of Fe^{3+} complexes which dissociate in the excited state to yield Fe^{2+} and an oxidized ligand (Sima and Makanova, 1997)

$$[Fe^{3+}(OH)]^{2+} + h\nu \rightarrow Fe^{2+} + HO^{\bullet} \tag{54}$$

$$[Fe^{3+}(RCOO)]^{2+} + h\nu \rightarrow Fe^{2+} + CO_2 + R^{\bullet} \tag{55}$$

Photo-Fenton techniques are useful since even at low [Fe^{3+}] high reaction rates are obtained. Besides, mineralization may be achieved through the photolysis of stable ferric complexes.

3.7.1 Influence of reaction conditions

The photo-Fenton degradation of NBE was studied under different conditions using simulated solar irradiation (Carlos et al., 2009). The induction period preceding the catalytic

phase is significantly shortened since the rates of the initial slow phase are enhanced by irradiation, although the effect of simulated solar light on the rates of the fast phase is negligible. The enhancement of the slow phase may be explained taking into account the contribution of photoinduced processes, such as the photoreduction of Fe^{3+} in the predominant Fe^{3+}–aquo complex at pH 3 by inner-sphere ligand-to-metal charge transfer (LMCT) (Lopes et al., 2002). At early stages, rxn (54) provides an alternative Fe^{3+} reduction pathway that is faster than rxn (45), thus substantially increasing Fe^{2+} and $HO^{\bullet}$ production rates. By contrast, the rates associated to the fast phase are independent of irradiation since they are mainly governed by thermal reactions (46) and (47). The effect of the initial concentrations on NBE and H_2O_2 profiles are shown in Fig. 8.

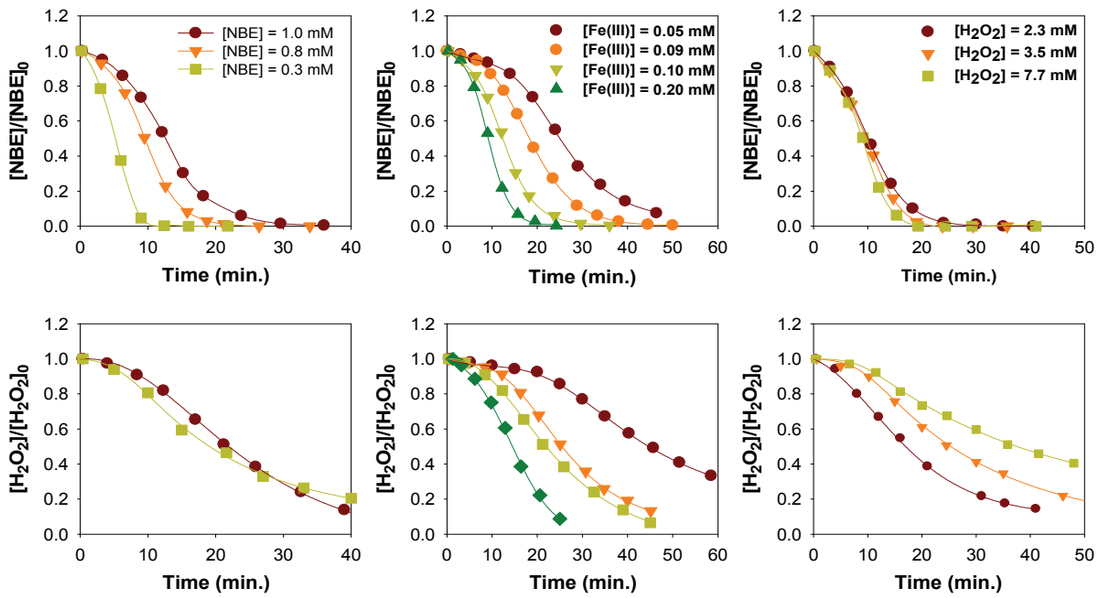

Fig. 8. Effect of initial conditions on the concentration profiles obtained during NBE photo-Fenton treatment.

In line with the results shown in section 3.6.1, the rates of the slow phase increase with $[Fe^{+3}]$ and $[H_2O_2]$, whereas z^{NBE}_{slow} values decreases with organic matter loading.

3.7.2 Influence of substrate structure

Degradation of the substrates of section 3.6.3 was studied under identical conditions but using UV irradiation (Fig. 9) (Nichela et al., 2010). As in the case of NBE, the slow initial phase is shortened in irradiated systems. The comparison between the different substrates reveals the same reactivity order as observed for Fenton-like systems. The solid lines in Fig. 9 confirm the utility of eqn (53) for describing autocatalytic profiles.

3.7.3 Photoenhancement factor

With the purpose of making a rough estimation of the relative contribution of photo stimulated pathways in photo-Fenton systems, we proposed (Nichela et al., 2010) the parameter photo enhancement factor (PEF) defined by

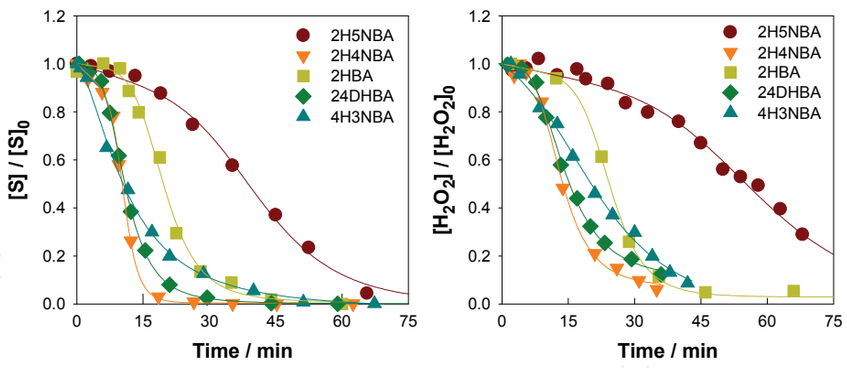

Fig. 9. Normalized concentration profiles of model substrates obtained in the photo-Fenton process.

$$PEF = \frac{k_{App}^{Phot} - k_{App}^{Dark}}{k_{App}^{Phot}} \tag{56}$$

where k^{Dark}_{App} and k^{Phot}_{App} are the rate constants linked to the dark and photo enhanced reactions, respectively. The PEF is a useful index that allows evaluating the contribution of photo induced processes in photo-Fenton systems. In addition, the "apparent half-lives" can be used to define an "overall photo enhancement factor" (PEF_O) by the following relation

$$PEF_O = 1 - \frac{t_{1/2}^{Phot}}{t_{1/2}^{Dark}} \tag{57}$$

The analysis of PEF_O values corresponding to the normalized profiles showed that higher photo enhancements are found for conditions where the dark reaction is slower. This behavior may be interpreted assuming that the rates of the photo induced reactions mostly depend on the photon flux and do not significantly depend on the nature of the substrate or the reaction conditions. Therefore, for a relatively constant photochemical contribution, the slower the dark reaction is, the greater the effect of photoinduced pathways results.

4. Product yields and mechanism of nitrobenzene transformation

Nitrobenzene thermal degradation was investigated using Fenton´s reagent in several experimental conditions. This section deals with the analysis of the distributions of intermediate reaction products and the mechanisms of nitrobenzene decomposition.

4.1 Initial steps of NBE transformation

From the analysis of reaction products distributions as a function of NBE conversion degree, a mechanism was proposed for NBE degradation in AOP systems (Carlos et al., 2008). The first steps involve two main pathways: hydroxylation pathways which yield phenolic derivatives and the nitration pathway which yields 1,3-dinitrobenzene (scheme 1).

Hydroxyl radicals usually react with benzene derivatives by electrophilic addition to form hydroxycyclohexadienyl-like radicals (Walling, 1975; Oturan and Pinson, 1995) that can undergo different processes according to the reaction conditions (i.e. $[Fe^{2+}]$, $[H_2O_2]$, $[Fe^{3+}]$,

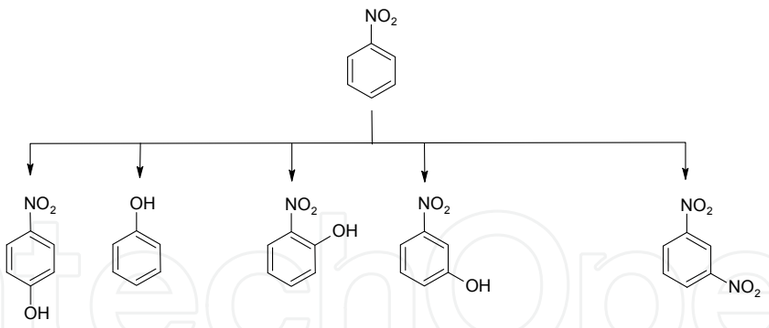

Scheme 1. Nitrobenzene primary hydroxylation and nitration pathways

$[O_2]$, etc.) (Pignatello et al., 2006). Since $HO^{\bullet}$ reacts with both the target substrate and its reaction products, the concentration profiles of reaction intermediates during AOP treatments result from a balance between their formation and degradation rates. As the composition of the reaction mixture changes with time, both the formation yields and degradation rates of intermediate products can vary during the course of reaction. Therefore, an important feature to be considered is the dependence of the mechanism with reagent concentrations since these parameters may influence the kinetics as well as the distribution of products thereby affecting the global efficiency of the detoxification process.

4.2 Analysis of primary product yields

The equations derived in section 2.3 were used to analyze the influence of reaction conditions on the primary reaction yields. The results are given below.

4.3 Hydroxylation Pathways

Normalized yields obtained in Fenton systems reveal significant differences in the product distributions associated to each reaction stage (Carlos et al., 2008). The η^{N}_{ONP} values observed during the initial fast phase are at least 30% lower than those determined in the slow one. On the contrary, η^{N}_{phenol} values are higher in the fast phase than in the slow one. In addition, increasing $[Fe^{2+}]_0$ markedly decreases η^{N}_{ONP} while significantly increases η^{N}_{phenol} values.

The observed differences in the normalized yields may be explained taking into account that the first oxidation step is the $HO^{\bullet}$ radical addition on the aromatic ring to form hydroxycyclohexadienyl-type radicals.

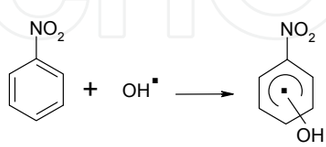

(58)

This type of radicals can undergo different reactions such as dimerization, disproportionation, oxygen addition to give corresponding peroxy-radical or can participate in electron transfer reactions with transition metals depending on the substituents in the aromatic ring and on the medium nature (Chen and Pignatello, 1997). The addition of $HO^{\bullet}$ radical in ortho, meta and para positions of the nitrobenzene ring can yield 2-nitrophenol (ONP), 3-nitrophenol (MNP) and 4-nitrophenol (PNP) by oxidation or disproportionation of the corresponding $HNCHD^{\bullet}$ radicals (Bathia, 1975)

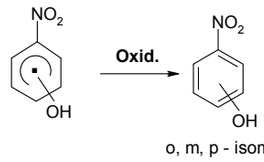

(59)

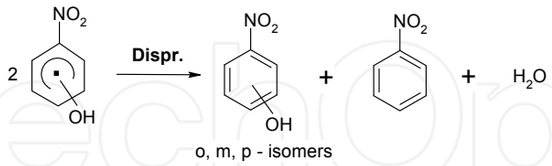

(60)

Usually, the distribution of isomers in HO• mediated hydroxylation does not obey the foreseen orientation according to deactivating characteristics of the nitro group but it depends significantly on reaction conditions.

4.3.1 Effect of O_2

In the presence of oxygen the second-order reactions have a secondary contribution to the primary phenolic yields, since HNCHD• radicals rapidly decay following a pseudo first order kinetics by addition of O_2. The oxidation of HNCHD• radicals by O_2 is a very complex process and several pathways leading to different reaction products can compete (Pan et al., 1993). Among the reaction routes involving the peroxyl radicals formed by O_2 addition to HNCHD•, the elimination of HO_2• yields the corresponding nitrophenols. Hence, [O_2] plays an important role in NBE degradation pathways. In the absence of O_2, bimolecular processes become significant. Our results suggest that in crossed disproportionation reactions, meta-HNCHD• radicals may act as oxidizers with respect to para-HNCHD• or ortho-HNCHD• radicals, yielding PNP or ONP and NBE (rxn (60)).

4.3.2 Effect of Fe^{2+}

The low ONP yields obtained with high [Fe^{2+}] can be explained by considering two consecutive processes, i.e. the selective reduction of ortho-HNCHD• radicals by Fe^{2+} to give Fe^{3+} and the corresponding organic anion followed by the regeneration of the starting nitrobenzene

$$\mathbf{Fe^{2+} + {\cdot}OHC_6H_5NO_2 \rightarrow C_6H_5NO_2 + Fe^{3+} + OH^-} \quad (61)$$

4.3.3 Effect of Fe^{3+}

The tests carried out in air saturated solutions show an increase of η^{N}_{ONP} with the [Fe^{3+}]. Since it is well known that Fe^{+3} is not a strong oxidant in aromatic hydroxylation (Fang et al., 1996), the increase of ONP yield with $[Fe^{3+}]_0$ can be explained if it is assumed that ortho-HNCHD• radicals are stabilized by means of Fe^{3+} complexation through one of the oxygen atoms belonging to the nitro group and the oxygen of the HO group. Within this context, the relatively high stability of ortho-NHCHD• radicals complexed with Fe^{3+} ions would allow explaining the observed results.

4.3.4 Phenol production

The presence of traces of phenol and NO_2^- among the initial reaction products shows that a small fraction of HO• radicals attacks the nitrobenzene ipso position and induces the

cleavage of the nitro group. The experimental results showed that the increase of [Fe^{2+}] is accompanied by an increase of phenol yiled. Therefore, phenol may be formed from nitrobenzene through rxn (62)

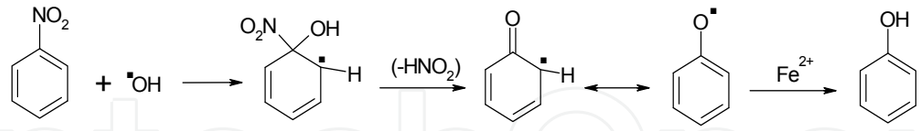

(62)

4.4 Nitration Pathways

As NBE degradation proceeds in AOP systems, the organic nitrogen is mainly released as nitrite ions (García Einschlag et al., 2002b; Carlos et al., 2008; Carlos et al., 2009). In the darkness and at pH 3, the released HNO_2/NO_2^- (pKa = 3.3) can lead to the formation of different nitrating agents such as peroxynitrous acid (ONOOH) and the $^{\bullet}NO_2$ radical through the following reactions (Fischer and Warneck, 1996; Merenyi et al., 2003):

$$\mathbf{HNO_2 + H_2O_2 + H^+ \rightarrow ONOOH + H_2O + H^+} \qquad \mathbf{k_{HOONO}} \tag{63}$$

$$\mathbf{HNO_2/NO_2^- + {}^{\bullet}OH \rightarrow {}^{\bullet}NO_2 + H_2O/HO^{\bullet}} \qquad \mathbf{k_{NO2-}} \tag{64}$$

The ONOOH decomposes in acid media yielding NO_3^-/H^+ and $^{\bullet}NO_2$/ $HO^{\bullet}$. Therefore, $^{\bullet}NO_2$ radicals can be in situ formed by NO_2^- oxidation trough either thermal or photochemical reactions. On the other hand, in UV/I systems both HNO_2/NO_2^- and NO_3^- photolysis may also contribute to the production of reactive nitrogen species through the photolytic reactions (34), (35), (36) and (38) (Mack and Bolton, 1999; Goldstein and Rabani, 2007). $^{\bullet}NO_2$ and ONOOH are nitrating agents capable of participating in the formation of 1,3-DNB under the reaction conditions used in the different AOPs.

In this section we analyze the conditions that favor the formation of 1,3-DNB during NBE treatment using different AOPs (Carlos et al., 2010). Fig. 10 plots the amount of 1,3-DNB formed (expressed as $[1,3\text{-DNB}]/[NBE]_0$) against the conversion degree of nitrobenzene (defined by $1\text{-}[NB]/[NBE]_0$). In all cases, the production of 1,3-DNB is practically negligible for NBE degradation percentages lower than 20%. Subsequently, the formation of 1,3-DNB increases until reaching a maximum for conversion degrees of about 0.9. Finally, as NBE is completely consumed, a steady decrease in 1,3-DNB concentration is observed. The latter trend is consistent with the hypothesis that 1,3-DNB is a primary product of NBE degradation (Carlos et al., 2008). It is important to note that, although curves in Fig. 10 show similar trends of 1,3-DNB formation, UV/H_2O_2 process yielded much lower 1,3-DNB levels than Fenton systems, thus suggesting an important contribution of iron species in NBE nitration pathways.

4.4.1 Influence of HNO_2/NO_2^- and NO_3^- in dark processes

NBE degradation experiments using Fenton's reagent in the dark and with different initial concentrations of NO_2^- or NO_3^- show that the presence of NO_3^- does not affect the consumption of NBE nor the production of 1,3-DNB while the presence of NO_2^- decreases NBE consumption and significantly increases the fraction of NBE transformed to 1,3-DNB. The latter trends can be explained by considering the enhancement, through rxn (64) of both $HO^{\bullet}$ radical scavenging and $^{\bullet}NO_2$ production as $[NO_2^-]_0$ is increased. Taking into account

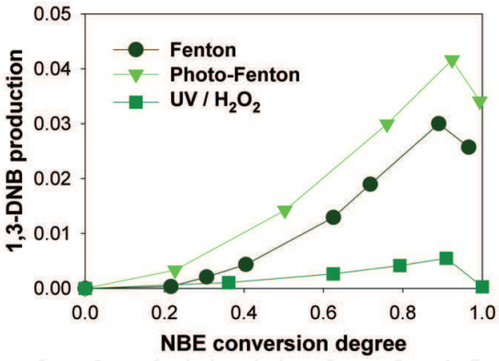

Fig. 10. Relative production of 1,3-dinitrobenzene against the conversion degree of nitrobenzene.

these results, the feasibility of a direct reaction between NBE and $^{\bullet}NO_2$ was tested by incubating NBE in solutions of HNO_2 at acid pH. In the latter conditions HNO_2 decomposes yielding $^{\bullet}NO_2$, $^{\bullet}NO$ and H_2O (Vione et al., 2005). Since [NBE] remained constant and no formation of 1,3-DNB was observed the direct reactions of either $^{\bullet}NO_2$ or $^{\bullet}NO$ with NBE were neglected.

4.4.2 Influence of HNO_2/NO_2^- and NO_3^- in photochemical processes

NBE degradation experiments were conducted at pH 3 in both UV/HNO_2/NO_2^- and UV/NO_3^- systems using different additive concentrations (García Einschlag et al., 2009). In UV/HNO_2/NO_2^- systems DNB yield ($\eta^0_{1,3\text{-DNB}}$) was negligible below 1mM of $[NO_2^-]_0$, then increased up to a value of 0.06 and remained constant above 8mM of $[NO_2^-]_0$. On the other hand, in UV/NO_3^- systems significant amounts of 1,3-DNB were observed even for very low $[NO_3^-]$ and $\eta^0_{1,3\text{-DNB}}$ increased with $[NO_3^-]$, 1,3-DNB being the most important by-product at high NO_3^- concentrations.

4.4.3 Influence of Fe^{3+} and O_2 in UV/HNO_2/NO_2^- and UV/NO_3^- systems

An enhancement of 1,3-DNB formation upon Fe^{3+} addition was observed in UV/HNO_2/NO_2^- systems. The increase of 1,3- DNB production with increasing $[Fe^{3+}]_0$ in UV/HNO_2/NO_2^- systems was explained by considering the production of $^{\bullet}NO_2$ through the sequence of reactions (54) and (64). In contrast, the presence of Fe^{3+} in UV/NO_3^- systems significantly increased NBE consumption rate while strongly decreased $\eta^0_{1,3\text{-DNB}}$. The latter result may be explained by taking into account: (i) an enhanced contribution of NBE oxidation pathways since higher production rates of nitrophenol isomers were observed, and (ii) the decrease of the relative importance of reactions (36) and (38) due to the lower fraction of photons absorbed by NO_3^-. In addition, UV/NO_3^- systems in the absence of O_2 showed $\eta^0_{1,3\text{-DNB}}$ values higher than those obtained under oxygenated conditions.

4.4.4 Nitration mechanism of NBE under mild AOP conditions

The set of results presented in section 4.4 is consistent with a nitration pathway involving a $HO^{\bullet}$ + $^{\bullet}NO_2$ mechanism. In the experimental domain tested, the prevailing NBE nitration pathway is most probably the reaction between the $^{\bullet}$OH-NB adduct and $^{\bullet}NO_2$ radicals (rxn 65A).

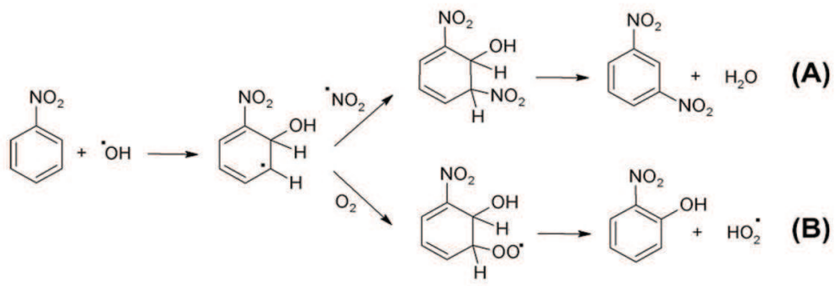

(65)

5. Conclusions

It is well known that rather complex reaction manifolds with many reaction steps are involved in the degradation of aromatic pollutants. However, results obtained in degradation experiments of nitroaromatic compounds using different homogeneous AOPs can be analyzed by using simplified models that take into account only a reduced number of kinetically key steps. These models are capable of correctly describing the main kinetic features of the studied systems by using only a few parameters as predictive tools. This kind of approach has important implications from a practical-technological viewpoint since it may be used for the rational design of efficient processes.

6. Acknowledgements

This work was partially supported by the project X559 of UNLP (Argentina). Daniela Nichela thanks the CONICET for a grant supporting her Ph.D. thesis. Luciano Carlos and Fernando García Einschlag are members of CONICET. The authors want to thank to the research groups of Prof. André M. Braun (University of Karlsruhe), Prof. Edmondo Pramauro (University of Turin) and Prof. Esther Oliveros (University Paul Sabatier of Toulouse) for the kind collaborations. Fernando García Einschlag is especially grateful for the support received from Prof. Dr. André M. Braun and Prof. Dr. Esther Oliveros throughout his research career.

7. References

Bathia, K., 1975. Hydroxyl radical induced oxidation of nitrobenzene. Journal of Physical Chemistry 79, 1032-1038.

Braun, A.M., Maurette, M.T., Oliveros, E., 1986. Photochemical Technologies. J. Willey & Sons., New York.

Buxton, G.V., Greenstock, C.L., Helman, W.P., Ross, A.B., 1988. Critical review of rate constants for reactions of hydrated electrons, hydrogen atoms and hydroxyl radicals in aqueous solution. J. Phys. Chem. Ref. Data 17, 513-886.

Carlos, L., Fabbri, D., Capparelli, A.L., Bianco Prevot, A., Pramauro, E., García Einschlag, F., 2009. Effect of simulated solar light on the autocatalytic degradation of nitrobenzene using Fe3+ and hydrogen peroxide. Journal of Photochemistry and Photobiology A: Chemistry 201, 32-38.

Carlos, L., Fabbri, D., Capparelli, A.L., Prevot, A.B., Pramauro, E., Einschlag, F.S.G., 2008. Intermediate distributions and primary yields of phenolic products in nitrobenzene degradation by Fenton's reagent. Chemosphere 72, 952-958.

Carlos, L., Nichela, D., Triszcz, J.M., Felice, J.I., García Einschlag, F.S., 2010. Nitration of nitrobenzene in Fenton's processes. Chemosphere 80, 340-345.

Crittenden, J.C., Hu, S., Hand, D.W., Green, S.A., 1999. A kinetic model for H2O2/UV process in a completely mixed batch reactor. Water Research 33, 2315-2328.

Chan, K.H., Chu, W., 2003. Modeling the reaction kinetics of Fenton's process on the removal of atrazine. Chemosphere 51, 305-311.

Chen, R., Pignatello, J.J., 1997. Role of quinone intermediates as electron shuttles in fenton and photoassisted fenton oxidations of aromatic compounds. Environmental Science and Technology 31, 2399-2406.

De Laat, J., Gallard, H., 1999. Catalytic decomposition of hydrogen peroxide by Fe(III) in homogeneous aqueous solution: Mechanism and kinetic modeling. Environmental Science and Technology 33, 2726–2732.

Fang, X., Mark, G., Sonntag, C.v., 1996. OH· radical formation by ultrasound in aqueous solutions Part I: The chemistry underlined the terephtalate dosimeter Ultrason. Sonochem. 3, 57-63.

Fischer, M., Warneck, P., 1996. Photodecomposition of nitrite and undissociated nitrous acid in aqueous solution. Journal of Physical Chemistry 100, 18749-18756.

García Einschlag, F.S., Carlos, L., Capparelli, A.L., 2003. Competition kinetics using the UV/H2O2 process: A structure reactivity correlation for the rate constants of hydroxyl radicals toward nitroaromatic compounds. Chemosphere 53, 1-7.

García Einschlag, F.S., Carlos, L., Capparelli, A.L., Braun, A.M., Oliveros, E., 2002a. Degradation of nitroaromatic compounds by the UV-H2O2 process using polychromatic radiation sources. Photochemical and Photobiological Sciences 1, 520-525.

García Einschlag, F.S., Felice, J.I., Triszcz, J.M., 2009. Kinetics of nitrobenzene and 4-nitrophenol degradation by UV irradiation in the presence of nitrate and nitrite ions. Photochemical and Photobiological Sciences 8, 953-960.

García Einschlag, F.S., Lopez, J., Carlos, L., Capparelli, A.L., Braun, A.M., Oliveros, E., 2002b. Evaluation of the efficiency of photodegradation of nitroaromatics applying the UV/H2O2 technique. Environmental Science and Technology 36, 3936-3944.

Getoff, N., 1997. Peroxyl radicals in the treatment of waste solutions. Peroxyl Radicals, 483-506.

Glaze, W.H., Lay, Y., Kang, J.W., 1995. Advanced oxidation processes. A kinetic model for the oxidation of 1,2-dibromo-3-chloropropane in water by the combination of hydrogen peroxide and UV radiation. Industrial and Engineering Chemistry Research 34, 2314-2323.

Goldstein, S., Lind, J., Merenyi, G., 2005. Chemistry of peroxynitrites as compared to peroxynitrates. Chemical Reviews 105, 2457-2470.

Goldstein, S., Rabani, J., 2007. Mechanism of nitrite formation by nitrate photolysis in aqueous solutions: The role of peroxynitrite, nitrogen dioxide, and hydroxyl radical. Journal of the American Chemical Society 129, 10597-10601.

Heit, G., Neuner, A., Saugy, P.-Y., Braun, A.M., 1998. Vacuum-UV (172 nm) Actinometry. The Quantum Yield of the Photolysis of Water. Journal of Photochemistry and Photobiology A: Chemistry 102, 5551-5561.

Lipczynska-Kochany, E., Bolton, J.R., 1991. Flash photolysis/HPLC method for studying the sequence of photochemical reactions: applications to 4-chlorophenol in aerated aqueous solution. Journal of Photochemistry and Photobiology, A: Chemistry 58, 315-322.

Lopes, L., De Laat, J., Legube, B., 2002. Charge transfer of iron(III) monomeric and oligomeric aqua hydroxo complexes: Semiempirical investigation into photoactivity. Inorganic Chemistry 41, 2505-2517.

Lopez, J.L., García Einschlag, F.S., González, M.C., Capparelli, A.L., Oliveros, E., Hashem, T.M., Braun, A.M., 2000. Hydroxyl radical initiated photodegradation of 4-chloro-3,5-dinitrobenzoic acid in aqueous solution. Journal of Photochemistry and Photobiology A: Chemistry 137, 177-184.

Mack, J., Bolton, J.R., 1999. Photochemistry of nitrite and nitrate in aqueous solution: A review. Journal of Photochemistry and Photobiology A: Chemistry 128, 1-13.

Mark, G., Korth, H.G., Schuchmann, H.P., Von Sonntag, C., 1996. The photochemistry of aqueous nitrate ion revisited. Journal of Photochemistry and Photobiology A: Chemistry 101, 89-103.

Merenyi, G., Lind, J., Czapski, G., Goldstein, S., 2003. Direct determination of the Gibbs' energy of formation of peroxynitrous acid. Inorganic Chemistry 42, 3796-3800.

Nadezhdin, A., Dunford, H.B., 1979. Oxidation of nicotinamide adenine dinucleotide by hydroperoxyl radical. A flash photolysis study. Journal of Physical Chemistry 83, 1957-1961.

Nichela, D., Carlos, L., Einschlag, F.G., 2008. Autocatalytic oxidation of nitrobenzene using hydrogen peroxide and Fe(III). Applied Catalysis B: Environmental 82, 11-18.

Nichela, D., Haddou, M., Benoit-Marquiè, F., Maurette, M.T., Oliveros, E., García Einschlag, F.S., 2010. Degradation kinetics of hydroxy and hydroxynitro derivatives of benzoic acid by fenton-like and photo-fenton techniques: A comparative study. Applied Catalysis B: Environmental 98, 171-179.

Oturan, M.A., Pinson, J., 1995. Hydroxylation by electrochemically generated OH · radicals. Mono- and polyhydroxylation of benzoic acid: Products and isomers' distribution. Journal of Physical Chemistry 99, 13948-13954.

Pan, X., Schuchmann, M.N., von Sonntag, C., 1993. Oxidation of benzene by the OH radical. A product and pulse radiolysis study in oxygenated aqueous solution. Journal of the Chemical Society, Perkin Transactions 2 3, 289-297.

Pignatello, J.J., Liu, D., Huston, P., 1999. Evidence for an additional oxidant in the photoassisted Fenton reaction. Environmental Science and Technology 33, 1832-1839.

Pignatello, J.J., Oliveros, E., MacKay, A., 2006. Advanced oxidation processes for organic contaminant destruction based on the fenton reaction and related chemistry. Critical Reviews in Environmental Science and Technology 36, 1-84.

Sima, J., Makanova, J., 1997. Photochemistry of iron (III) complexes. Coordination Chemistry Reviews 160, 161-189.

Simic, M., 1975. The chemistry of peroxy radicals and its implication to radiation biology. Fast Processes in Radiation Chemistry and Biology, 162-179.

Stefan, M.I., Bolton, J.R., 1998. Mechanism of the degradation of 1,4-dioxane in dilute aqueous solution using the UV/hydrogen peroxide process. Environmental Science and Technology 32, 1588-1595.

Stefan, M.I., Hoy, A.R., Bolton, J.R., 1996. Kinetics and mechanism of the degradation and mineralization of acetone in dilute aqueous solution sensitized by the UV photolysis of hydrogen peroxide. Environmental Science and Technology 30, 2382-2390.

Stefan, M.I., Mack, J., Bolton, J.R., 2000. Degradation pathways during the treatment of methyl tert-butyl ether by the UV/H2O2 process. Environmental Science and Technology 34, 650-658.

Vione, D., Maurino, V., Minero, C., Lucchiari, M., Pelizzetti, E., 2004. Nitration and hydroxylation of benzene in the presence of nitrite/nitrous acid in aqueous solution. Chemosphere 56, 1049-1059.

Vione, D., Maurino, V., Minero, C., Pelizzetti, E., 2005. Nitration and photonitration of naphthalene in aqueous systems. Environmental Science and Technology 39, 1101-1110.

Walling, C., 1975. Fenton's reagent revisited. Accounts of Chemical Research 8, 125-131.

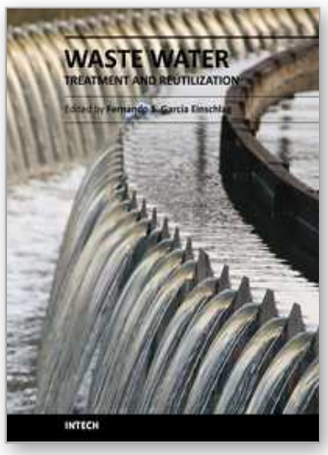

Waste Water - Treatment and Reutilization
Edited by Prof. Fernando SebastiÃ¡n GarcÃa Einschlag

ISBN 978-953-307-249-4
Hard cover, 434 pages
Publisher InTech
Published online 01, April, 2011
Published in print edition April, 2011

The steady increase in industrialization, urbanization and enormous population growth are leading to production of huge quantities of wastewaters that may frequently cause environmental hazards. This makes waste water treatment and waste water reduction very important issues. The book offers a collection of studies and findings concerning waste water treatment, minimization and reuse.

How to reference
In order to correctly reference this scholarly work, feel free to copy and paste the following:

Fernando S. García Einschlag, Luciano Carlos and Daniela Nichela (2011). Degradation of Nitroaromatic Compounds by Homogeneous AOPs, Waste Water - Treatment and Reutilization, Prof. Fernando SebastiÃ¡n GarcÃa Einschlag (Ed.), ISBN: 978-953-307-249-4, InTech, Available from: http://www.intechopen.com/books/waste-water-treatment-and-reutilization/degradation-of-nitroaromatic-compounds-by-homogeneous-aops

INTECH
open science | open minds

InTech Europe
University Campus STeP Ri
Slavka Krautzeka 83/A
51000 Rijeka, Croatia
Phone: +385 (51) 770 447
Fax: +385 (51) 686 166
www.intechopen.com

InTech China
Unit 405, Office Block, Hotel Equatorial Shanghai
No.65, Yan An Road (West), Shanghai, 200040, China
中国上海市延安西路65号上海国际贵都大饭店办公楼405单元
Phone: +86-21-62489820
Fax: +86-21-62489821

IntechOpen